

## MCST Internal Memo

**Date:** November 3<sup>rd</sup>, 2023

**From:** Tiejun Chang, Ashish Shrestha, Carlos Perez Diaz, Hanzhi Lin, Aisheng Wu, Yonghong Li, Na Chen, and Truman Wilson

**To:** MODIS Science Team members

**Subject:** Proposed calibration improvements for the MODIS thermal emissive bands in Collection 7 Level 1B processing

**Memo #:** 1163.1

### 1. INTRODUCTION

This document summarizes the calibration improvements for the MODIS thermal emissive bands (TEBs) in Collection 7 (C7) Level 1B (L1B) as proposed by the MODIS Characterization Support Team (MCST). This version (#1163.1) is an update to the original memo (#1163.0) released on December 11, 2020.

#### 1.1 MODIS TEBs Collection 6.1

The current MODIS Collection 6.1 (C6.1) look-up table (LUT) on-orbit update algorithms for the Terra and Aqua MODIS TEBs are summarized in Table 1.1-1 [1]. The band 21  $b_1$  linear coefficient (not described in Table 1.1-1) is derived using the on-board blackbody (BB) cooldown (CD) data - with the offset and non-linear calibration terms constrained to zero in the fitting algorithm. The Terra MODIS photoconductive (PC) longwave infrared (LWIR) TEBs crosstalk coefficients were derived using lunar observation analyses from the mission beginning. Moreover, an electronic crosstalk correction is applied to Terra MODIS photovoltaic (PV) LWIR bands 27-30 during calibration and Earth-view (EV) retrievals. The Aqua C6.1 MODIS TEBs use the pre-launch  $a_0$  with instrument temperature adjustment for PV bands and  $a_0=0$  for PC bands and pre-launch adjusted  $a_2$  calibration coefficients for all bands – except for bands 31 and 32 ( $a_0$  is equal to zero and  $a_2$  is derived using the CD data) [2]. In a general sense, brightness temperature (BT) difference analyses between the current LUT and newly derived  $a_0$  and  $a_2$  calibration coefficients are performed to verify if a forward LUT update of the calibration algorithm coefficients is necessary. If the update criteria are exceeded, a LUT update is issued to meet the radiometric accuracy requirements of the L1B data in forward production.

Additional LUTs are updated on an as needed basis for the MODIS C6.1 TEBs. These include those used to calculate the time-dependent uncertainty index (UI) - updated after every calibration coefficients LUT update, the time-dependent quality assessment (QA) LUT, and the Aqua default  $b_1$  LUT.

Table 1.1-1 Terra and Aqua MODIS C6.1 TEBs calibration algorithms.

(PL: pre-launch; CD: cooldown)

Band	Aqua	Terra	
	Calibration algorithm	Calibration algorithm	Cross-talk correction
20	PL $a_0$ PL adjusted CD $a_2$	$a_{0\_ms1} = 0$  $a_{0\_ms2} =$ $a_{0\_ms2}^{free-fit} -$ $a_{0\_ms1}^{free-fit}$  CD $a_2$	PV LWIR electronic cross-talk
22			
23			
24			
25			
27			
28			
29			
30			
31	$a_0=0$ , CD $a_2$	$a_0 = 0$  CD $a_2$	PC LWIR optical cross-talk
32			
33	$a_0=0$ PL adjusted CD $a_2$		
34			
35			
36			

## 1.2 C7 algorithm improvements

Several calibration algorithm improvements were discussed, tested, validated, and are hereby proposed by MCST in preparation for C7. These are listed below, and the recommended MODIS C7 LUT update algorithms for the Terra and Aqua MODIS TEBs are summarized in Table 1.2-1 and Table 1.2-2. Detailed algorithm descriptions for Terra and Aqua MODIS are presented in Sections 3 and 4, respectively.

### A. Terra MODIS TEBs

- (1) MWIR bands crosstalk correction for selected detectors for calibration and EV measurements
- (2) Early mission PC bands  $a_0$  correction to reduce the mirror side difference
- (3) Bands 20 and 29  $a_0$  adjustment from MODIS-IASI comparison and qDCC assessment decrease cold scene bias
- (4) Nonlinear coefficient  $a_0$  and  $a_2$  improvement for calibration stability for Band 30
- (5) Electronic crosstalk coefficient uncertainty and propagation to L1B data uncertainty for MWIR and PV LWIR bands

B. Aqua MODIS TEBs

- (1) MWIR crosstalk correction for selected detectors for calibration and EV measurements
- (2) LWIR bands crosstalk correction for calibration and EV measurements
- (3) Mission-long  $a_0$  correction and  $a_2$  update using BB CD data for improvement on mirror side consistence and long-term stability for PV bands
- (4) PV LWIR bands nonlinear coefficient  $a_2$  improvement to stability improvements
- (5) Electronic crosstalk coefficient uncertainty and propagation to L1B data uncertainty for MWIR and PV LWIR bands

Table 1.2-1 Terra MODIS C7 TEBs calibration algorithms recommendations with comparison with C6.1. (MS: mirror side; PL: pre-launch; CD: cold-down)

Band	Terra C6.1		Terra C7			
	Calibration algorithm	Crosstalk correction (for calibration and EV)	Calibration algorithm	Crosstalk correction (for calibration and EV)		
20	$a_{0\_ms1} = 0$  $a_{0\_ms2} =$ $a_{0\_ms2}^{free-fit} -$ $a_{0\_ms1}^{free-fit}$  CD $a_2$	PV LWIR electronic cross-talk	Corrected $a_0$ ; CD $a_2$	Electronic cross-talk corrections for selected detectors		
22			$a_{0\_ms1} = 0$ $a_{0\_ms2} =$ $a_{0\_ms2}^{free-fit} - a_{0\_ms1}^{free-fit}$		CD $a_2$	
23						
24			Corrected $a_0$ ; CD $a_2$	PV LWIR electronic cross-talk		
25						
27			$a_0 = 0$  CD $a_2$		PC LWIR optical cross-talk	MS Corrected $a_0$ CD $a_2$ ; Fixed after 003
28						
29						
30						
31	$a_0 = 0$  CD $a_2$	PC LWIR optical cross-talk	$a_0 = 0$ CD $a_2$	PC LWIR optical cross-talk		
32						
33						
34						
35						
36						

Table 1.2-2 Aqua MODIS C7 TEB calibration algorithm recommendations compared to C6.1. (MS: mirror side; PL: prelaunch; CD: cooldown)

Band	Aqua C6.1		Aqua C7	
	Calibration algorithm	Crosstalk correction (for calibration and EV; post safe mode only)	Calibration algorithm	Crosstalk correction (for calibration and EV)
B20, 22-25	PL $a_0$ PL adjusted CD $a_2$	Crosstalk correction for all detectors + EV adjusted	PL $a_0$ with MS correction CD $a_2$	Crosstalk correction for select detectors
27			PL $a_0$ with MS correction CD $a_2$ Cold scene-based $a_0$ correction	Crosstalk correction for all detectors + EV adjusted
28				Crosstalk correction for all detectors starting 2012 + EV adjusted
29				Crosstalk correction for all detectors + scaled by time-dependent factor across mission + EV adjusted
30			PL $a_0$ with MS correction No $a_2$ change since 2012036 Cold scene-based $a_0$ correction	Crosstalk correction for all detectors + EV adjusted
31, 32	$a_0 = 0$ , CD $a_2$		$a_0 = 0$ , CD $a_2$	
33-36	$a_0 = 0$ PL adjusted CD $a_2$		$a_0 = 0$ PL adjusted CD $a_2$	

## 2. MODIS TEB CALIBRATION ALGORITHM BACKGROUND

### 2.1 MODIS TEB calibration algorithm

MODIS TEB includes mid-wave infrared (MWIR) bands 20-25, covering a wavelength range from 3.8 to 4.5  $\mu\text{m}$ , and long-wave infrared (LWIR) bands 27-36, from 6.8 to 14.2  $\mu\text{m}$ . All the MWIR and LWIR bands 27-30 consist of ten PV detectors per band, while the LWIR bands 31-36 consist of ten PC detectors per band. The on-board BB serves as the primary calibration source, while the space view (SV) provides an instrument background reference. Normally, this temperature is set to 290 K and 285 K for Terra and Aqua MODIS, respectively. Starting in April 2020, the Terra BB temperature setpoint has been changed to 285 K. The MODIS TEBs calibration uses a quadratic calibration algorithm on a scan-by-scan basis for each TEB detector and scan-mirror side. The linear coefficient of the response function is calibrated scan-by-scan using a two-point calibration performed via the response to the on-board BB referenced to the SV, and the non-linear and offset terms coming from a LUT. The BB warm-up and cooldown (WUCD) operation is used to characterize and update the

instrument non-linear response coefficients on-orbit. Every WUCD operation is performed quarterly, and the BB temperature varies from instrument ambient temperature (about 270 K) to 315 K. The calibration radiance ( $L_{CAL}$ ) from the BB view is defined as:

$$L_{CAL} = RVS_{BB}\varepsilon_{BB}L_{BB} + (RVS_{SV} - RVS_{BB})L_{SM} + RVS_{BB}(1 - \varepsilon_{BB})\varepsilon_{cav}L_{cav}, \quad (1)$$

where  $\varepsilon$  is the BB or cavity (cav) emissivity,  $L$  is the radiance for the BB, scan mirror (SM), or cavity, and RVS is the response-versus-scan-angle at the SV or BB view. The TEB calibration is based on a quadratic algorithm that converts the digital response of the sensor to calibration radiance ( $L_{CAL}$ ):

$$L_{CAL} = a_0 + b_1dn_{BB} + a_2dn_{BB}^2, \quad (2)$$

where  $a_0$  and  $a_2$  are the offset and non-linear coefficients, and  $dn_{BB}$  is the BB's digital response. Equations (1) and (2) are used for both the WUCD and scan-by-scan linear coefficient calibrations during nominal operation. The scan-by-scan linear coefficient,  $b_1$ , can be calculated using the emissivity, RVS, and nonlinear coefficients LUTs:

$$b_1 = [L_{CAL} - a_0 - a_2dn_{BB}^2]/dn_{BB}. \quad (3)$$

Using the calibration coefficients for each detector and scan mirror side, EV radiance retrievals can be calculated by:

$$L_{EV} = \frac{1}{RVS_{EV}} [a_0 + b_1dn_{EV} + a_2dn_{EV}^2 - (RVS_{SV} - RVS_{EV})L_{SM}], \quad (4)$$

where  $RVS_{EV}$  is the EV RVS as a function of mirror AOI. The MODIS TEBs RVS come from pre-launch tests and have been verified and monitored post-launch using pitch maneuvers. A detailed description on the MODIS TEB calibration is described by Xiong et al. [1].

The calibration assessment can be performed using L1B data over selected Earth scenes. Since the on-board BB temperature is from approximately 270K to 315K, the  $a_0$  uncertainty is relatively large and thus the  $a_0$  uncertainty has larger impact on the measurement over cold scenes. Deep convective clouds (DCC) have been proven to be useful Earth scenes for the calibration assessment of the MODIS TEBs. In order to remove solar reflectance effects on the measurements of MWIR bands and assess the calibration at low BTs, Quasi-deep convective clouds (qDCC), which are the DCC during nighttime, are used [6]. From the MODIS TEB calibration algorithm, the calibration uncertainty impact on the L1B product can be modeled analytically. A detailed description on the development and application of this technique to DCC is described by Chang et al. [6]. One practical application is to use the model to evaluate mirror side, detector, or bias differences. It can also be utilized to assess long-term stability. Thus, the calibration uncertainty impact on the L1B product can be modeled, and an  $a_0$  correction for mirror side or bias differences can be derived.

## 2.2 MODIS TEBs electronic crosstalk

Signal contamination in the form of electronic crosstalk has been observed in many of the TEBs since pre-launch. This became particularly evident for Terra MODIS bands 27 – 30 after the instrument underwent a safe mode event in February 2016, for which a correction was applied in C6.1 shortly after [3, 4]. Moreover, some of the detectors in the Terra MODIS MWIR bands also show signs of electronic crosstalk contamination, which can be seen clearly from the Moon observations. The signal contamination for band 22 detector 8 and sending signal alignment with the contamination for band 23 detector 10 is illustrated in Fig. 2.2-1. Several anomalous peaks due to contamination from detectors in bands 20, 21, 23, 24 and 26 outside of the main lunar signal, which is cut off at the top of Figs. 2.2-1a and 2.2-1b, can be easily seen. These anomalous peaks represent crosstalk contamination. Furthermore, these electronic crosstalk effects can potentially impact the L1B and higher-level products, causing image artifacts such as striping and radiometric biases.

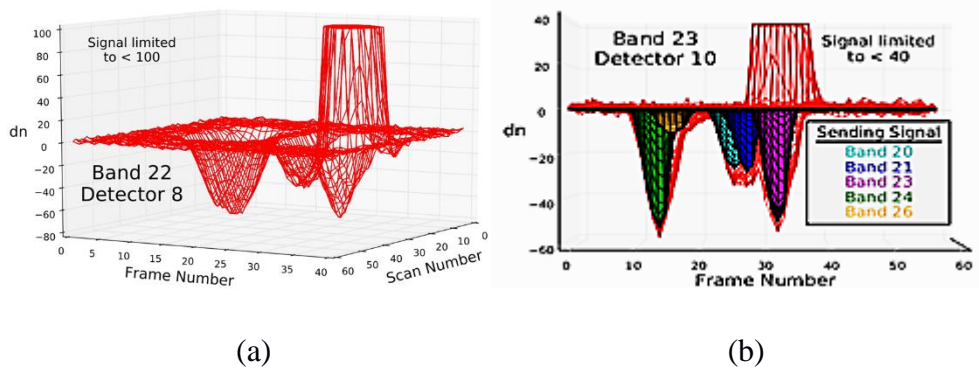


Figure 2.2-1: Example of contamination data around the main lunar signal. The data for these plots are from the Terra MODIS lunar observation on May 26, 2016.

Generally, crosstalk occurs between bands and detectors that are located on the same FPA (Fig. 2.2-2). The source of the contaminating signals can be identified using lunar data. There are two kinds of crosstalk. One is detector 1 contamination from detector 10 of a sending band, as shown in Fig. 2.2-2 (a). The second is band-to-band among MWIR bands or among PV LWIR bands, as shown in Fig. 2.2-2 (b). The contaminating signal has been assumed to be linearly proportional to the measured signal from the identified sending bands. Since electronic crosstalk affects the digital signal in each data sector, it will have an impact on background signal as well as the signal from any measured EV or on-board calibrator (OBC) scene. However, since the background contamination is at a nearly constant level, this contamination can be subtracted off with the rest of the background signal. In a simplistic fashion, the crosstalk coefficients,  $c_{i,j}$ , are in the form of a matrix which contains linear coefficient values that connect a detector's receiving contamination ( $i$ ), to each of the detectors that send contamination ( $j$ ). The correction is applied to the background-subtracted digital counts ( $dn$ ) for each data sector in order to derive the calibration coefficients and EV scene radiance. Thus, the corrected signal on the pixel level can be written as:

$$dn_i(S, F) = dn_i^*(S, F) - \sum_j c_{i,j} dn_j^*(S, F + \Delta F_j) \quad (5)$$

Here,  $S$  and  $F$  represent the scan and frame numbers, respectively,  $\Delta F_j$  is the relative frame offset of detector  $j$  with respect to detector  $i$ , and the \* represents the digital counts before the application of the correction. A detailed description of the correction and its impact on the L1B data is described by Wilson et al. [4], and in the 2018 MODIS TEB electronic crosstalk workshop [5].

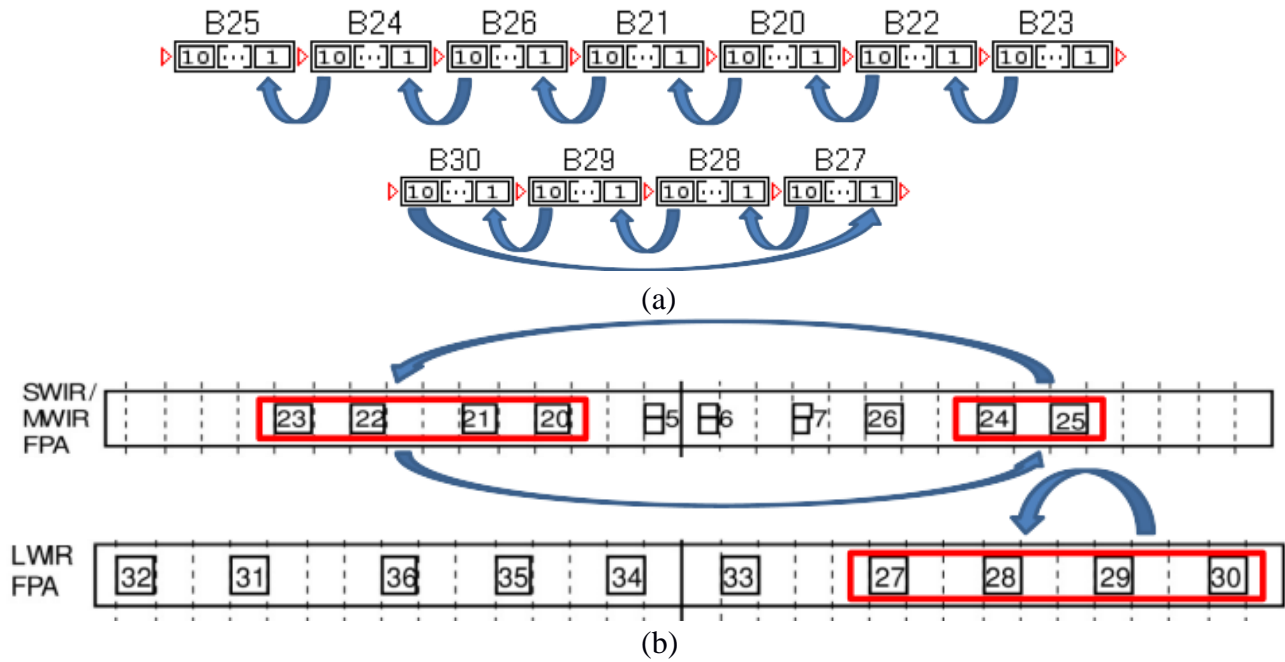


Figure 2.2-2: MODIS TEBs (a) detector-to-detector and (b) band-to-band crosstalk contamination schematic.

### 3. TERRA MODIS TEB C7 CALIBRATION IMPROVEMENTS

#### 3.1 MWIR electronic crosstalk correction

A crosstalk correction for selected detectors of the Terra MWIR bands will be applied in C7. Each detector that was selected for correction underwent extensive evaluation of the correction's impact on the L1B product and image quality. Figure 3.1-1 displays an example of the electronic crosstalk correction coefficients application on the L1B product for band 24. It can be clearly seen from the images, BT profiles, and BT histograms that the application of the electronic crosstalk coefficients effectively removes striping and brings the corrected detectors in-family with the other detectors. Ultimately, it was decided that only 4 detectors (band 22 detector 8, band 23 detectors 1 and 10, and band 24 detector 1) in the Terra MWIR bands have contamination levels that are significant enough to require a correction in the L1B product (Table 3.1-1). Figure 3.1-2 illustrates the Terra MODIS C7 MWIR electronic crosstalk correction coefficients mission-long trends for the selected detectors and bands, respectively. All other detectors have either small levels of contamination or the correction is

not significant enough - when compared to the normal variation of the bands' BT retrievals. These results and conclusions were presented in August 2018 in a workshop hosted by MCST at the MODIS Sensor Working Group (MsWG) meeting referred to as the MODIS Thermal Emissive Band Crosstalk Workshop [5].

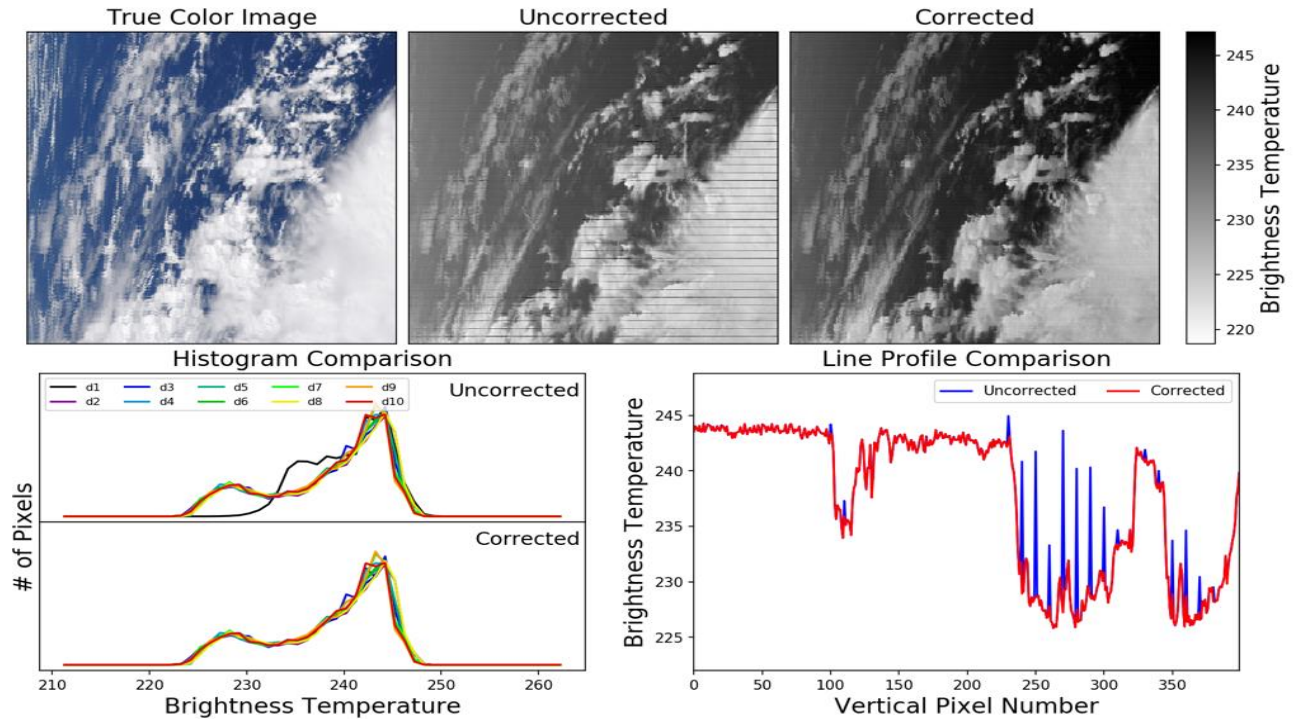


Figure 3.1-1: Crosstalk correction example for Terra MODIS band 24. (Top) True color, uncorrected, and corrected images. (Bottom left) Histogram comparisons for the selected scene before and after the electronic crosstalk correction is applied. (Bottom right) Vertical line profiles comparison through the center frame of the selected scene.

Table 3.1-1 Terra MODIS MWIR bands and detectors selected for electronic crosstalk correction in C7.

Band	Detector	Contamination Impact
22	8	Large striping over ice cloud scenes and water scenes (~0.5K).
23	1,10	Large striping over ice cloud scenes and water scenes (~0.5K).
24	1	Striping over ice cloud scenes and 0.5 -1 K change over ocean scenes

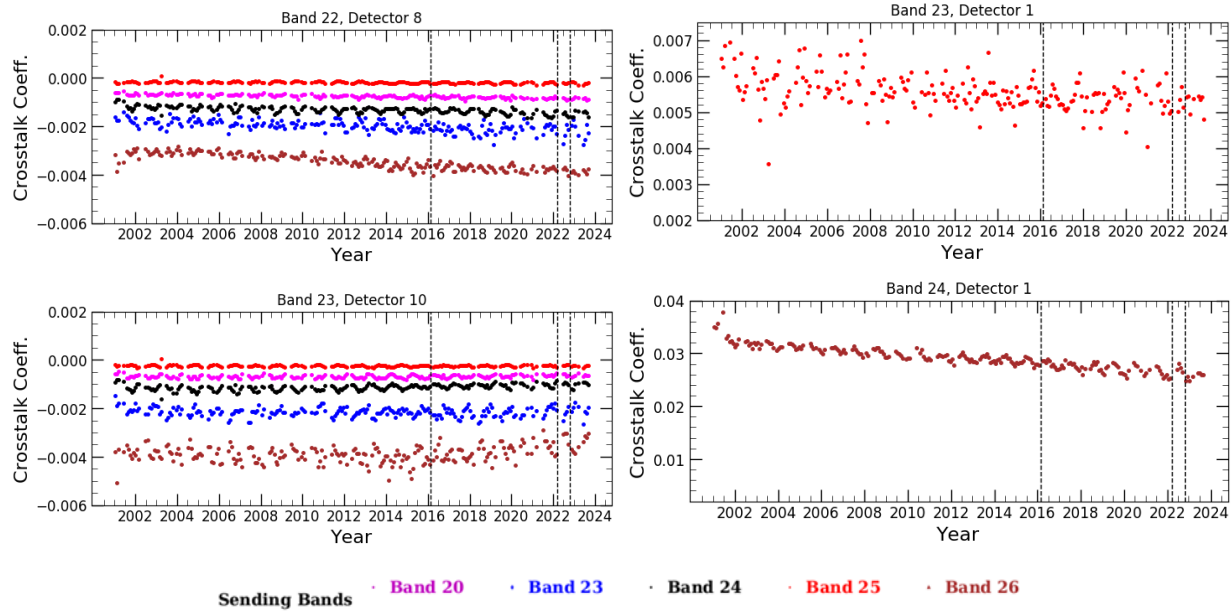


Figure 3.1-2: Terra MODIS C7 MWIR electronic crosstalk correction coefficients mission-long trends for the select detectors and bands.

### 3.2 Band 30 stability improvement

Inter-sensor comparisons and vicarious calibration approaches have confirmed that the Terra band 30 BTs have been drifting downward [7-11]. This has been observed both through the Terra MODIS-Infrared Atmospheric Sounding Interferometer (IASI) time series (2007-2019) and MODIS mission-long EV trending results over qDCC, Dome Concordia (Dome-C), and the ocean (Figs. 3.2-1 and 3.2-2). These biases are larger for lower BT scenes. To correct this artifact, for both the Dome-C site and an ocean location in the Bahamas, one month's worth of EV data for every year of the Terra MODIS mission was re-processed using the  $a_0$  and  $a_2$  calibration coefficients from the 2003 LUT after the instrument's last configuration change. Comparison tests between these coefficients and C6.1 demonstrated significant reduction in bias for both Earth scenes. Figure 3.2-3 illustrates the C7 bias corrections for the Dome-C and ocean targets. Thus, Terra MODIS C7 will use the  $a_0$  and  $a_2$  calibration coefficients from the 2003 LUT (after last configuration change) to re-process Terra MODIS band 30 for the instrument's entire mission. Moreover, the Dome-C, ocean, and qDCC Earth scenes will continue to be monitored for bias changes in C7.

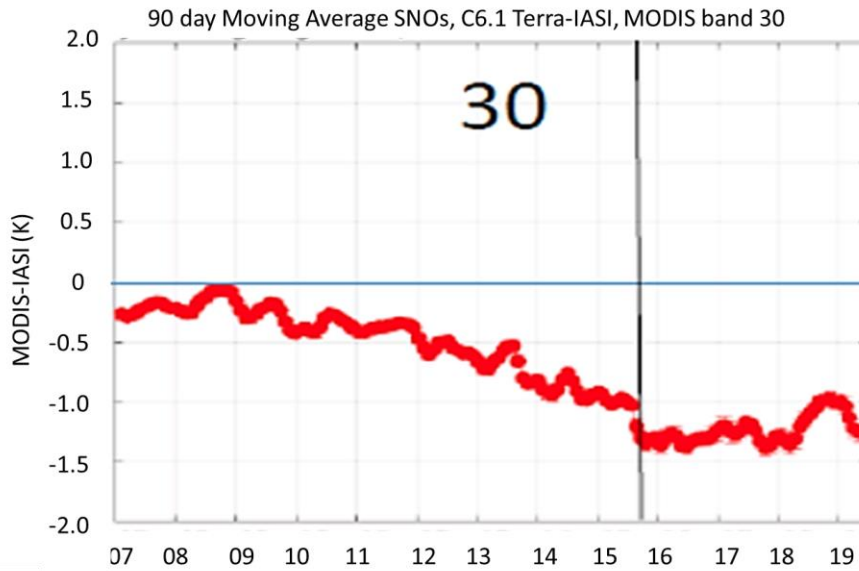


Figure 3.2-1. Terra MODIS-IASI biases for Terra MODIS band 30 from the years 2007 to 2019. This is for C6.1. (Source: Chris Moeller)

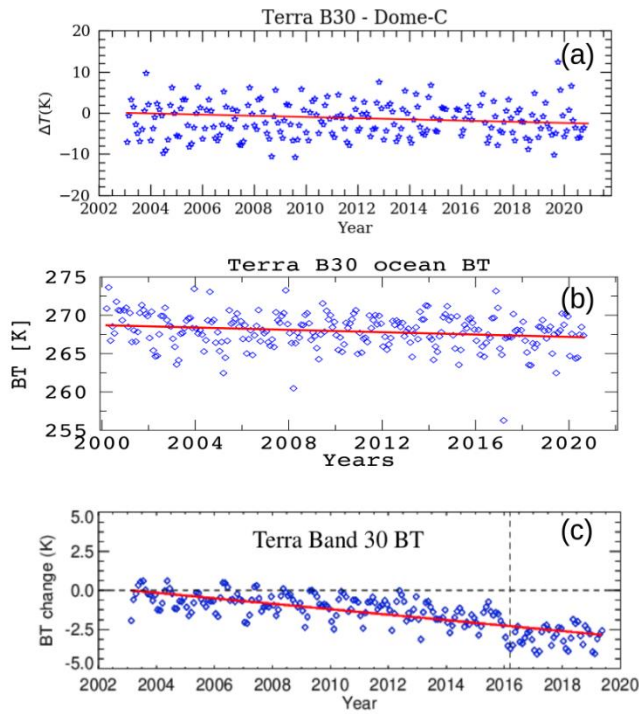


Figure 3.2-2. Terra MODIS mission-long retrievals over (a) Dome-C, (b) the ocean, and (c) qDCC for band 30. Blue markers represent monthly-averaged data. Red lines define the data's fit. This is for C6.1.

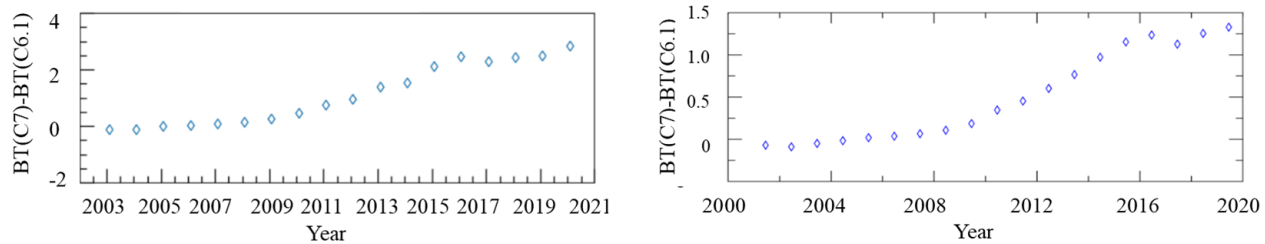
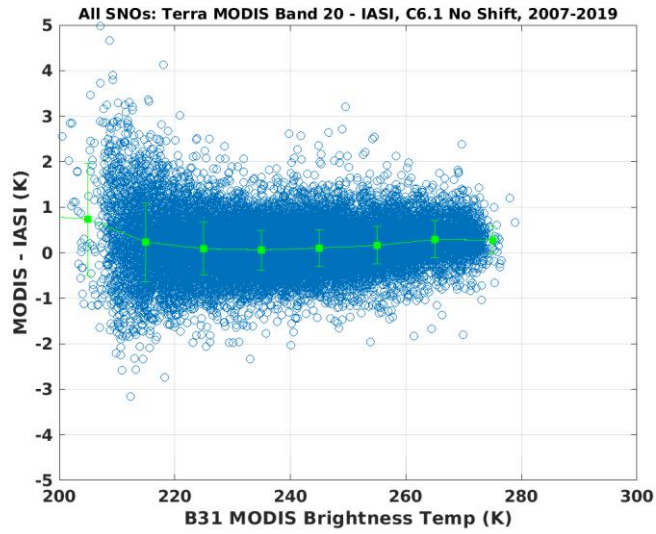


Figure 3.2-3. Terra MODIS C7 band 30 bias corrections (compared to C6.1) for the (left) Dome-C and (right) ocean targets. Blue markers represent monthly-averaged data.

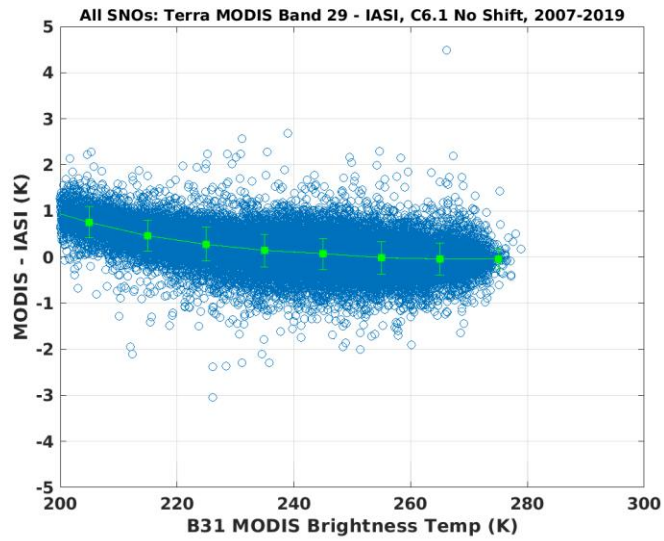
The C7 semi-L1B test for Dome-C shows residual differences between mirror sides and residual drift in the EV time series. An algorithm for an additional  $a_0$  correction was developed to reduce the mirror side difference. From the Dome-C residual mirror side difference assessment, additional time-dependent  $a_0$  corrections are calculated. Taking into account mirror side consistency, this  $a_0$  correction is applied to mirror side 1.

### 3.3 Bands 20 and 29 cold scene bias correction

When compared to the IASI instrument, part of the payload of the MetOp series of polar-orbiting meteorological satellites, Terra MODIS has shown cold scene biases for some TEBs, as demonstrated by Moeller et al. [7]. This has been further confirmed by MCST in separate efforts [8]. Figure 3.3-1 displays the cold scene biases for Terra MODIS bands 20 and 29 when compared to IASI from the years 2007 to 2019. For band 20, warm scenes show quite stable trends. However, band 29 shows a slight upward trend for the warmer scenes. In order to solve for these biases, a similar strategy to the one discussed in Section 2.3 was used, where the BT-dependent biases are estimated using the Terra MODIS-IASI difference at 200 K from 2007-2019, and the trends of the biases are obtained from MODIS retrievals over qDCC. Figure 3.3-2 illustrates the Terra MODIS mission-long retrievals over qDCC, Terra-IASI biases over qDCC, and  $a_0$  corrections for bands 20 and 29. Using the MODIS retrievals over qDCC referenced to the Terra-IASI biases, an  $a_0$  correction is derived for each month of data. This  $a_0$  correction, as well as the free-fitted  $a_2$ , are calculated using a yearly-averaged sliding window. Because Terra MODIS underwent several configurations and settings changes from the years 2000 to 2003, the average  $a_0$  correction from 2003-2004 is used for band 20 over this early mission period to avoid discontinuity. Moreover, after every WUCD operation, an  $a_0$  correction is applied to both mirror sides and  $a_2$  is computed. Before C7 is implemented, the Terra MODIS C6.1 qDCC trends and Terra-IASI biases will be processed to maintain continuous  $a_0$  corrections. After its implementation, the C7 L1B will be used to monitor the qDCC and bias trends. Furthermore, Dome-C, ocean, and desert measurements will also be used as a reference to monitor a broader BT range.



(a)



(b)

Figure 3.3-1. Terra MODIS-IASI biases for Terra MODIS bands (a) 20 and (b) 29 from the years 2007 to 2019. (Source: Chris Moeller)

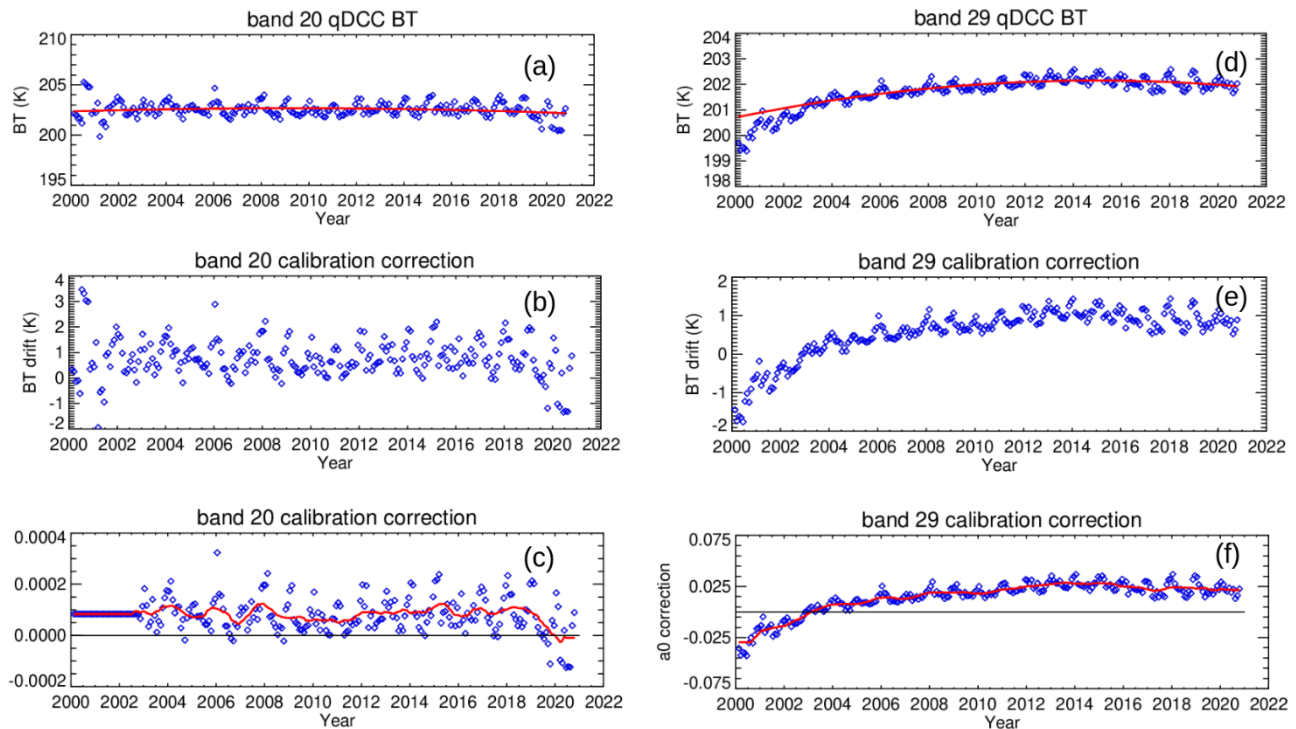


Figure 3.3-2. Terra MODIS mission-long retrievals over qDCC (a and d), Terra-IASI biases over qDCC (b and e), and  $a_0$  correction (c and f) for bands 20 and 29. Blue markers represent monthly-averaged data. Red lines define data's fit in (a) and (d) and yearly moving average in (c) and (f).

### 3.4 Early mission PC bands mirror side difference correction

Early in the Terra MODIS mission (2000-2002), the instrument underwent several instrument setting and electronic configuration changes (Table 3.4-1). Hence, the instrument response was affected after each change and, consequently, the calibration data shows relatively larger uncertainty when compared to that after the year 2003. The mirror side differences were analyzed for each TEB and each time interval between these changes, and assessments over qDCC and Dome-C show relatively larger mirror side differences and discontinuities for low BT measurements. MCST performed several analyses and found that re-processing the C7 LUTs to accommodate for new timestamps - more representative of each setting and configuration change - improves the calibration consistency and accuracy by generating LUTs for each change period. The PV bands mirror side differences were mostly reduced. However, because  $a_0$  is set to zero for both mirror sides for the PC bands, the mirror side differences remained. Figure 3.4-1 illustrates the Terra MODIS early mission mirror side BT differences for bands 34 (~0.5 K) and 36 (~0.8 K). Thus, MCST analyzed the mirror side BT differences using cold scenes and derived an  $a_0$  correction associated with the mirror side differences for PC bands 33-36. This  $a_0$  correction is used to generate the C7  $a_0$  and  $a_2$  LUTs between 2000 and 2003. Lastly, Fig. 3.4-2 shows the Terra MODIS mirror side BT difference comparison as a function of BT between C7 and C6.1 for bands 34 and 36 using the LUTs from the WUCD operation that happened on October 27<sup>th</sup>, 2001. The cross-comparison between C7 and C6.1 demonstrates mirror side BT difference corrections of 0.5 K and 0.7 K at 200K for bands 34 and 36, respectively.

Table 3.4-1. Terra MODIS setting and configuration changes from 2000 to 2002.

Date	Changes
06/08/00	Cold focal plane assembly stopped controlling temperature
10/30/00	MODIS switches to B-side electronics configuration
07/02/01	MODIS switches to A-side electronics configuration using PS1
03/19/02	Spacecraft safe mode anomaly during maneuver
09/17/02	Switch to B-side formatter; other components remain on A-side

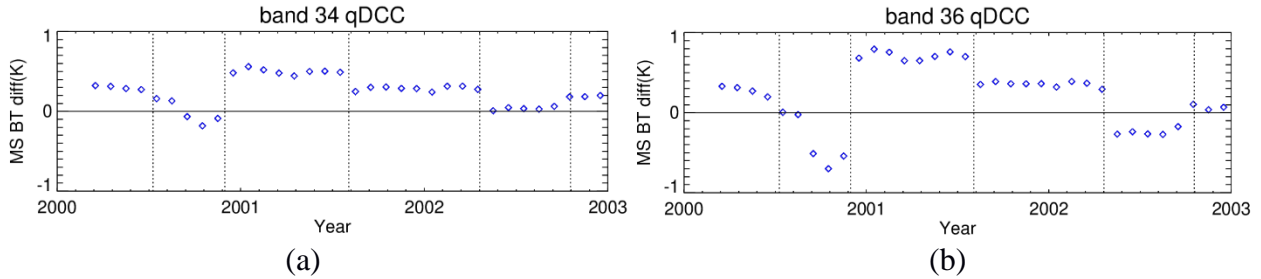


Figure 3.4-1. Terra MODIS early mission mirror side BT differences for bands (a) 34 and (b) 36. Blue markers represent monthly-averaged data.

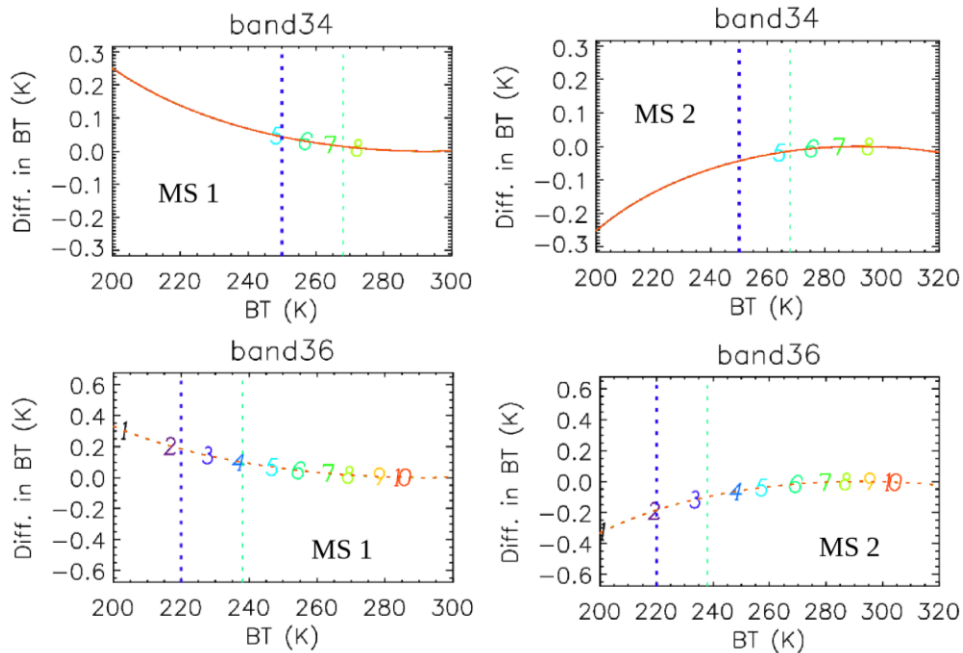


Figure 3.4-2. Terra MODIS mirror side BT difference comparison as a function of BT between C7 and C6.1 for bands 34 and 36 using the LUTs from the WUCD operation that happened on October 27<sup>th</sup>, 2001. The number and color indicate the detector number. The vertical dashed lines are for typical temperature and temperature at 0.3 typical radiance.

### 3.5 C7 uncertainty penalty

The contamination due to crosstalk contributes additional uncertainty. The uncertainty of the crosstalk coefficients and their fluctuation relative to the LUT value can propagate to the L1B product. In C7, the crosstalk coefficient uncertainty is derived from the fitting residuals between the measured values and a linear fit over a three-year sliding window.

The uncertainty of the crosstalk coefficients for each receiving detector propagates to the L1B data associated with this detector. A time-dependent uncertainty LUT is used for L1B processing. The uncertainty propagation for one receiving detector is the sum from all sending detectors. With the crosstalk coefficient uncertainty LUT, the uncertainty for a receiving detector due to the crosstalk is calculated as

$$unc = \frac{\sqrt{\sum_i (\Delta c_i * dn_i)^2}}{dn^*}, \quad (6)$$

where  $\Delta c$  is the crosstalk coefficient uncertainty from sending detector  $i$ ,  $[dn]_i$  is the sending detector's digital number, and  $[dn]^*$  is the crosstalk corrected digital number of the receiving detector. The sum is over all the sending detectors. The uncertainty associated with crosstalk is scene and BT dependent. It is calculated for each pixel in L1B products. The uncertainty due to crosstalk is combined with the other uncertainty contributions for the TEB L1B data uncertainty estimation. Same change was made for the Aqua C7 MODIS TEB.

## 4. AQUA MODIS TEB CALIBRATION IMPROVEMENTS

### 4.1 Aqua MWIR and LWIR electronic crosstalk correction

Aqua MODIS C7 will introduce electronic crosstalk correction coefficients for selected detectors in the MWIR bands and all detectors in the PV LWIR bands. Signatures of electronic crosstalk contamination are seen in lunar images by various Aqua MODIS bands from both the MWIR and LWIR FPAs. MCST spent substantial effort on surveying lunar images from scheduled lunar observations to determine all the bands and detectors affected by electronic crosstalk artifacts and linked these with their respective sending bands and detectors. Moreover, linear crosstalk correction coefficients were derived from Moon observations for the pertinent bands/detectors and the entire Aqua MODIS mission. Afterwards, these were used to generate corrected L1B images and assess the impacts of electronic crosstalk on imagery. A detailed description of the correction and its impact on the L1B data is described by Keller et al. [12,13].

After various analyses and tests on the electronic crosstalk correction impacts on the L1B product, MCST proposes to apply electronic crosstalk corrections to all detectors in the Aqua C7 PV bands. These results and conclusions were also presented in August 2018 in the MODIS Thermal Emissive Band Crosstalk Workshop [5]. Table 4.1-1 summarizes the MWIR bands selected for electronic crosstalk correction in Aqua MODIS C7. Figure 4.1-1 illustrates the Aqua MODIS C7 MWIR electronic crosstalk correction coefficients mission-long trends for the select detectors. Figure 4.1-2 illustrates the Aqua MODIS C7 band 30 electronic crosstalk correction coefficients mission-long trends.

Generally, all coefficients for the MWIR bands are stable throughout the entire Aqua MODIS mission. The coefficients for the PV LWIR bands show a slight downward trend starting around 2012 with a larger change following the 2022 safe mode. Lastly, Figures 4.1-3 and 4.1-4 show examples of the electronic crosstalk correction coefficients application on the L1B product for bands 24 and 30. The L1B images displayed correspond to granules from October 11<sup>th</sup>, 2019. The electronic crosstalk corrections are applied to detector 1 (product order (P.O.)) for all the Aqua MWIR bands described in Table 4.1-1. It can be inferred from the images, BT profiles, and BT histograms that the application of the electronic crosstalk coefficients effectively removes striping and brings detector 1 in-family with the other detectors for all bands (more apparent for band 24, whose electronic crosstalk coefficients are larger (~4%) than for the other bands (<2%)). In the case of Aqua PV-LWIR bands 27 to 30, the electronic crosstalk correction is applied for all detectors.

Table 4.1-1. Aqua MODIS MWIR band detectors selected for electronic crosstalk correction in C7.

Band	Detector	Contamination Impact
20	1	Striping over some scenes (~0.15K).
22	1	Striping over some scenes (~0.20K).
23	1	Large striping over ice cloud scenes and water scenes (~0.5K).
24	1	Striping over low BT scenes during daytime.
25	1	Striping over some scenes (~0.20K).

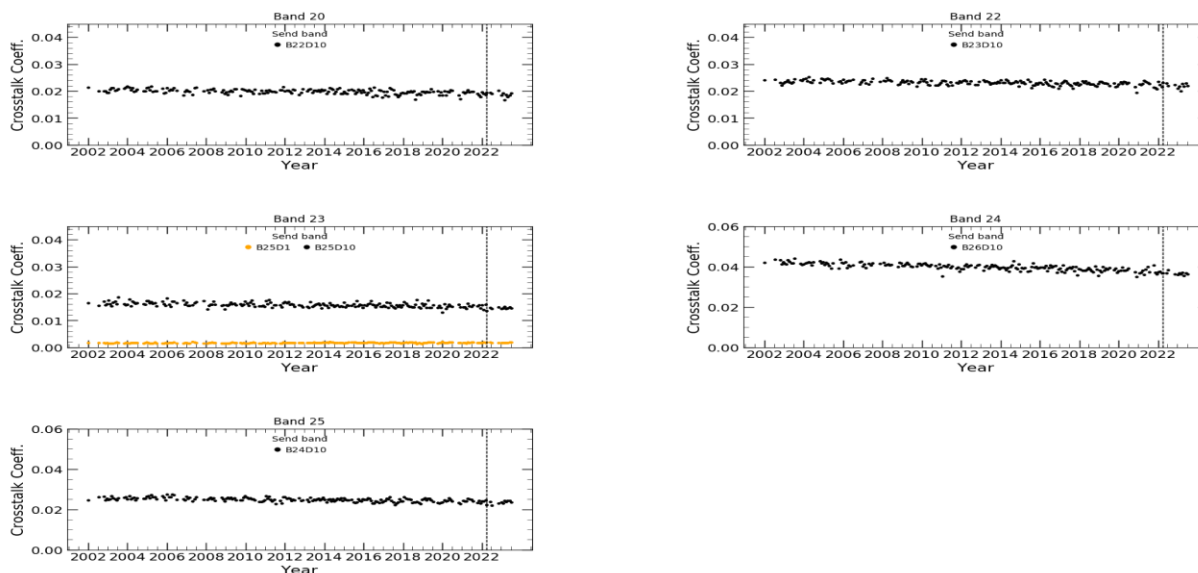


Figure 4.1-1. Aqua MODIS C7 electronic crosstalk correction coefficients mission-long trends for MWIR bands selected detectors.

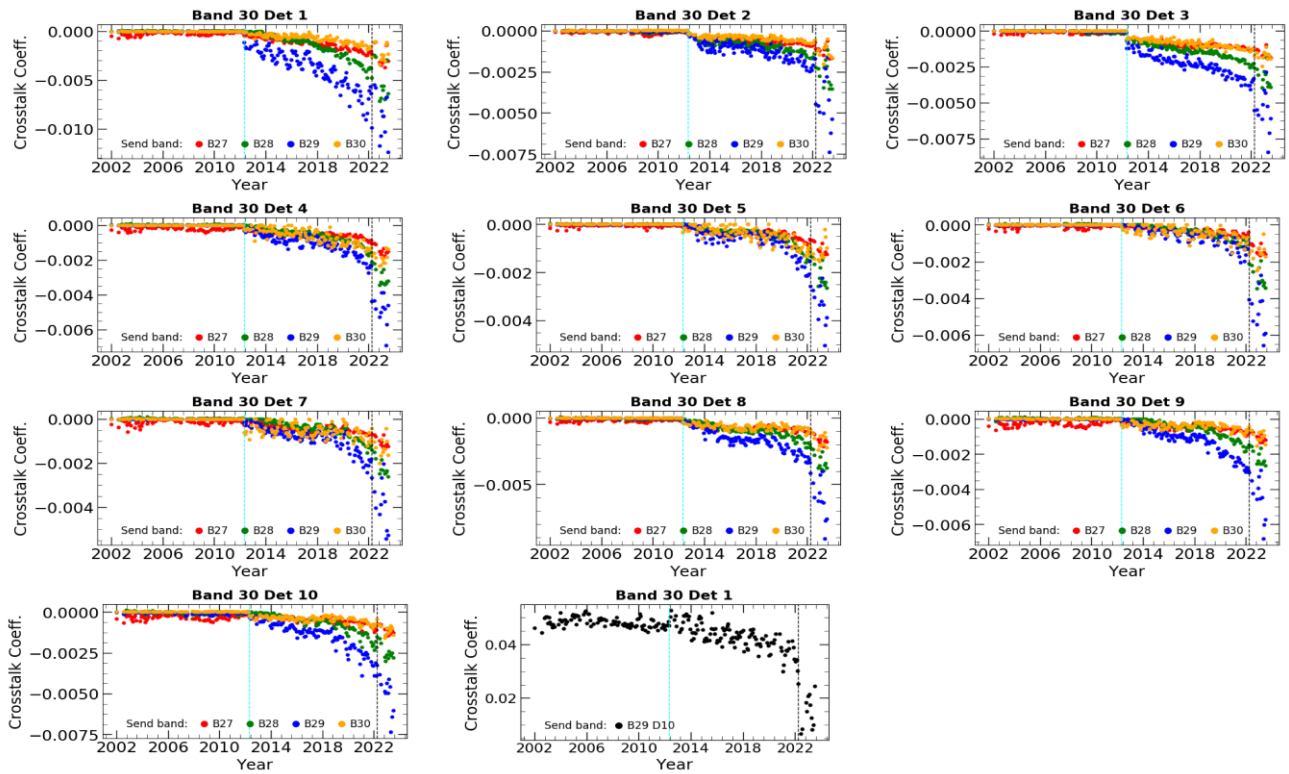


Figure 4.1.-2. Aqua MODIS electronic crosstalk correction coefficients mission-long trends for band 30.

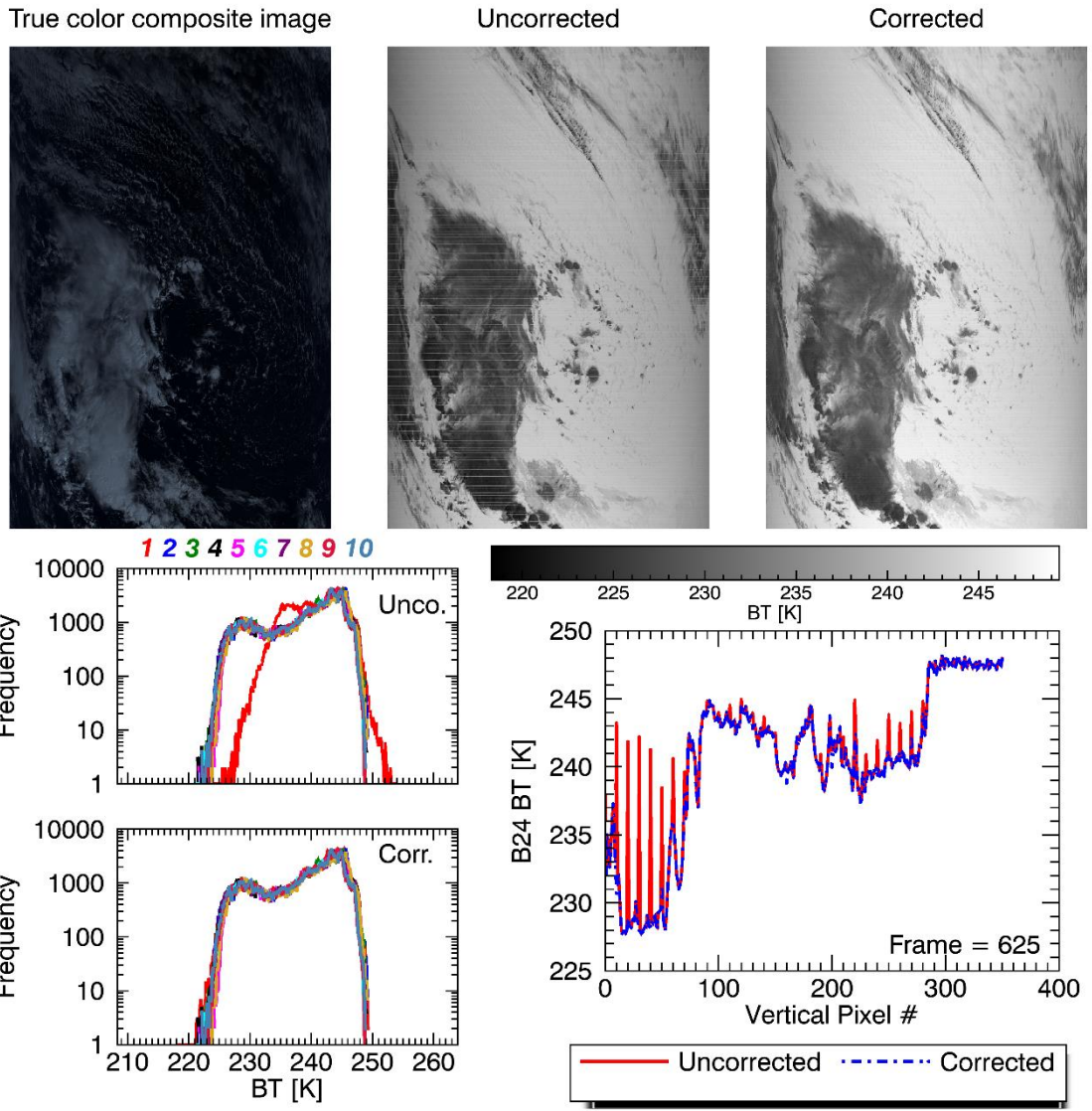


Figure 4.1-3. Electronic crosstalk correction coefficients application on the L1B product example for band 24, detector 1 (P.O.). The L1B images displayed correspond to a granule from October 11<sup>th</sup>, 2019.

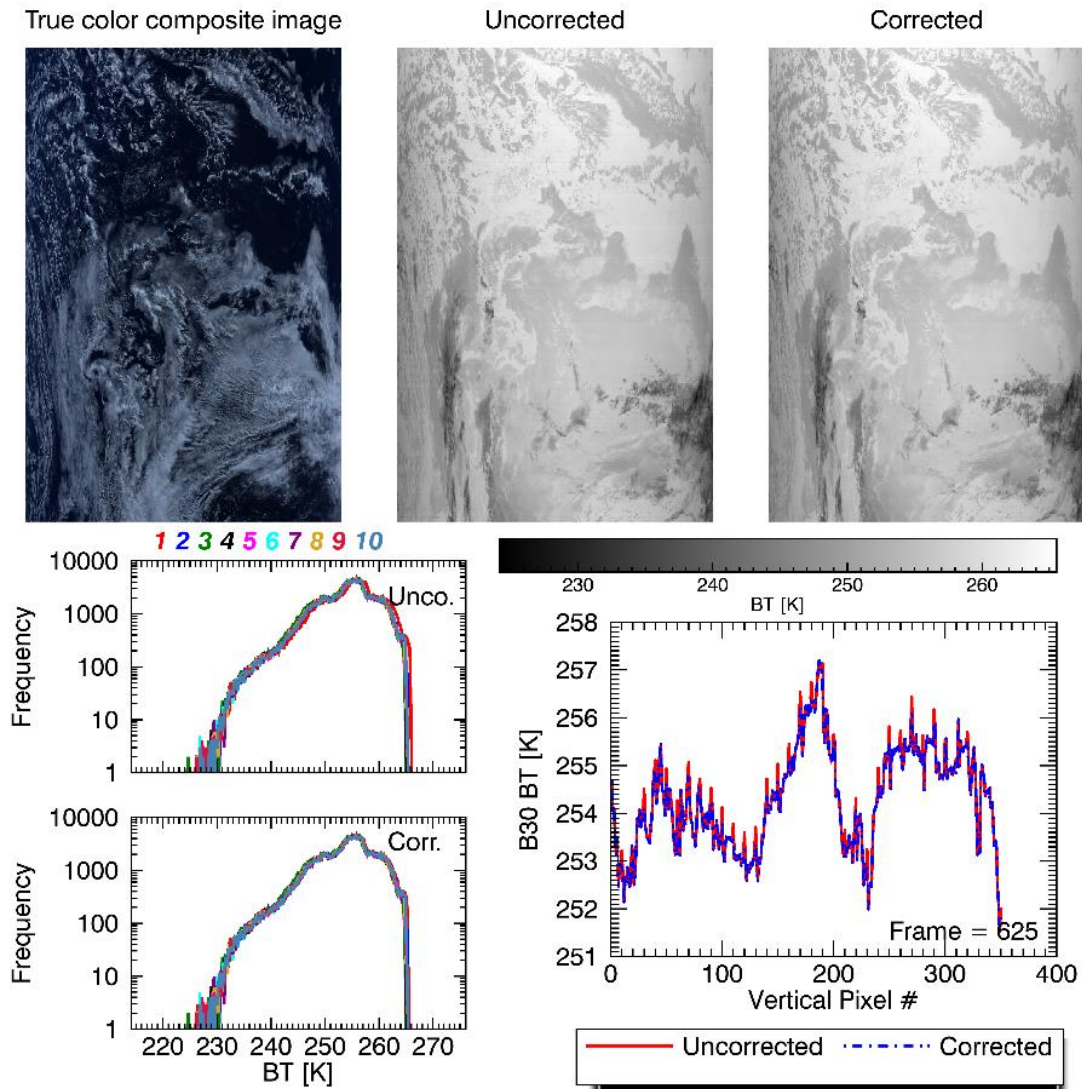


Figure 4.1-4. Electronic crosstalk correction coefficients application on the L1B product example for band 30, detector 1 (P.O.). The L1B images displayed correspond to a granule from October 11<sup>th</sup>, 2019.

#### 4.2 Electronic crosstalk coefficients adjustment using EV scenes

MCST found that after the Aqua MODIS EV scene images have been crosstalk corrected, residual striping remains. Thus, to provide a better L1B product, an EV-based adjustment to the crosstalk coefficients is made. The adjusted PV LWIR crosstalk coefficients are the product of Moon-derived crosstalk coefficients and an adjustment factor. The adjustment factor is used to correct for residual striping not corrected by the Moon-derived crosstalk coefficients which itself is calculated from an FFT analysis using one orbit's worth of data over EV scenes from a date closest to the lunar event. The Moon-derived crosstalk coefficients are receiving and sending band and detector specific, while the adjustment factors are only receiving band and detector specific. Figure 4.2-1 shows an example of the uncorrected (left), corrected (center), and adjusted corrected (right) images for Aqua MODIS

band 27. It can be observed that the EV-based adjustment reduces the striping and provides better overall image quality (albeit scene-dependent).

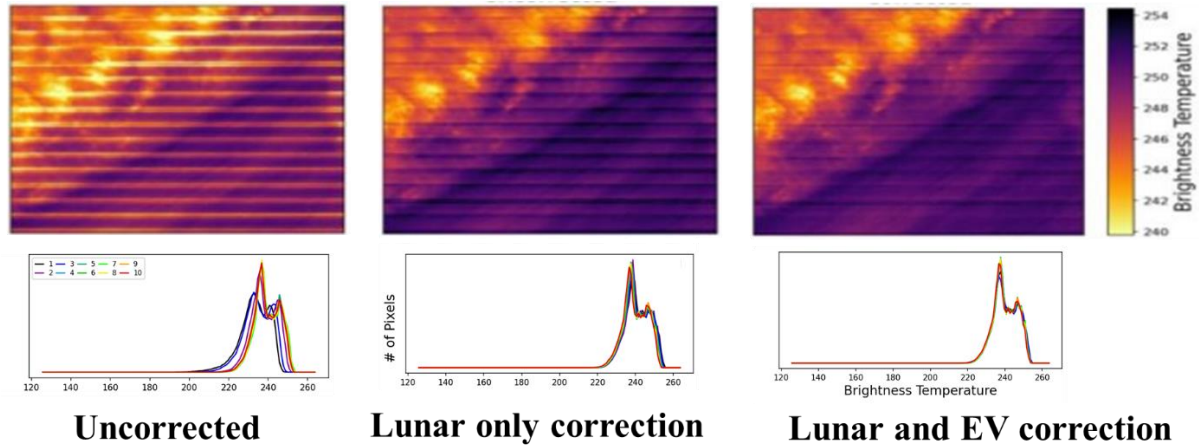


Figure 4.2-1. Same Aqua MODIS band 27 EV image uncorrected (left), corrected (center), and adjusted corrected (right).

### 4.3 Mission-long mirror side difference correction for PV bands

As shown in Table 1.1-1, the pre-launch  $a_0$  with instrument temperature adjustment is used for Aqua PV bands 20-25 and 27-30, while  $a_0$  is set to zero for PC bands 31-36. After the Aqua MODIS mission-long mirror side BT differences were analyzed using qDCC, the formatter reset event (January 2018) was found to have caused significant mirror side difference changes. Therefore, as the methodology presented in Section 2.3, qDCC were used to assess the instrument changes and associate the mirror side differences to an  $a_0$  correction. The method was applied to the MODIS PV bands (except band 21). Figure 4.3-1 illustrates the Aqua MODIS mission-long mirror side BT differences for MWIR bands 20-25. Band 20 has the largest mirror side BT difference (approximately 1.8 K) before the formatter reset. After the reset, this mirror side difference is significantly reduced (decreased to 0.5 K). The other MWIR TEBs also show up to a 1-K mirror side BT difference before the formatter reset event. Because band 21 uses a linear calibration algorithm with  $a_0$  and  $a_2$  set to zero, its mirror side BT differences are not directly comparable to the other bands. Before and after the formatter reset, the band 21 mirror side BT differences change direction. For all other TEBs, the mirror side differences are smaller after the reset.

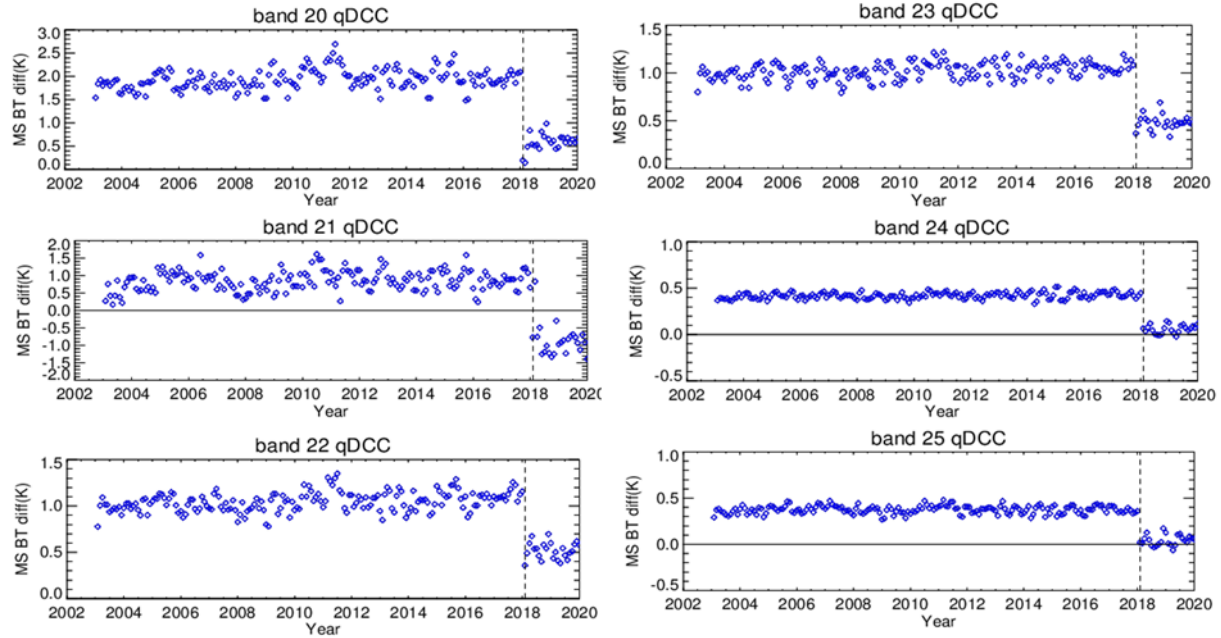


Figure 4.3-1. Aqua MWIR bands 20-25 long-term mirror side BT differences over qDCC. Each symbol represents monthly-averaged mirror side differences. The vertical dashed line indicates the time of occurrence for the formatter reset (January 2018).

Figure 4.3-2 displays the C6.1 Aqua MODIS mission-long mirror side BT differences for PV LWIR bands 27-30. Band 27 has the largest mirror side difference among these four bands (approximately 0.8 K) before the formatter reset. Similar to the MWIR TEBs, after the reset, the mirror side differences for all four bands decreased significantly. Moreover, all four bands exhibit slight - and similar in pattern - mirror side difference fluctuations, suggesting that these are not noise. The PC LWIR TEBs mirror side differences are small and not shown here. Figure 4.3-3 shows the Aqua mission-long  $a_0$  correction for all TEBs - except bands 21 and 31. A linear calibration is still applied to band 21 in C7, and thus the  $a_0$  correction is not applied to this band. Band 31 is used as the reference band for the qDCC pixel identification process; hence no mirror side differences and no  $a_0$  corrections are derived for this band. Moreover, band 31 exhibits accurate calibration and excellent stability. As such, its mirror side differences are expected to be negligible. The MODIS band 31 calibration accuracy and stability has been presented in some literatures.

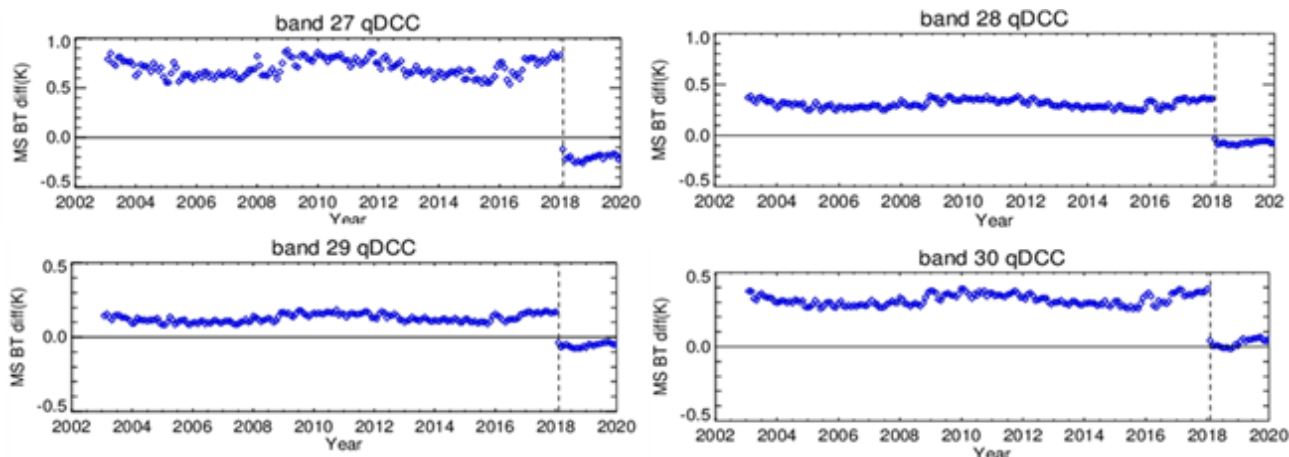


Figure 4.3-2. Aqua LWIR bands 27-30 long-term mirror side BT differences over qDCC. Each symbol represents the monthly-averaged mirror side differences. The vertical dashed line indicates the time of occurrence for the formatter reset (January 2018).

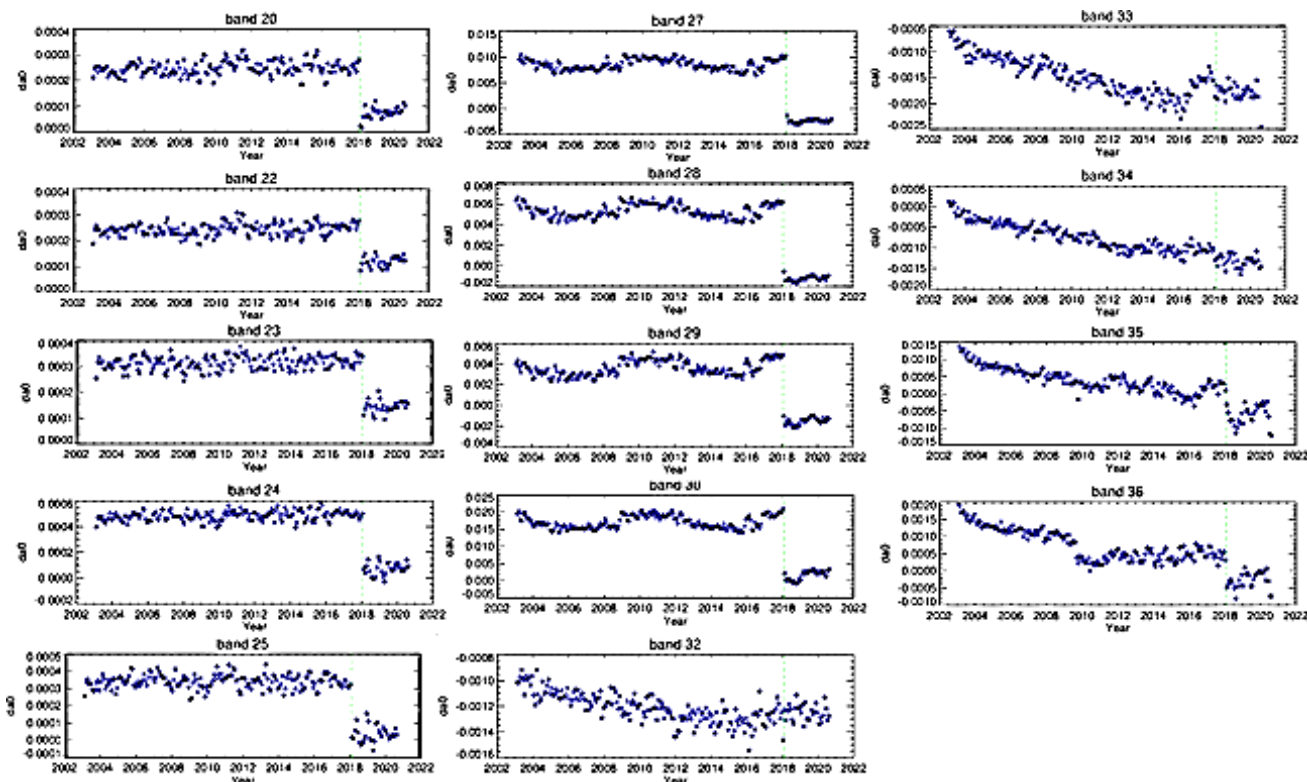


Figure 4.3-3. Aqua mission-long  $a_0$  correction (delta\_a0) for all TEBS. Each symbol represents the monthly  $a_0$  correction. The vertical dashed line indicates the time of occurrence for the formatter reset (January 2018).

After deriving the  $a_0$  bias correction using extremely cold scenes (i.e. qDCC), a set of test LUTs (later on referred to as C7) were developed to evaluate their efficacy in reducing the Aqua MODIS TEBs mirror side differences when compared to C6.1. The C7 algorithm was slightly changed to the one currently employed in C6.1 by applying the derived bias correction ( $+1/2$  to MS2,  $-1/2$  to MS1) to the pre-launch  $a_0$  coefficients and, afterwards, free-fitting the  $a_2$  coefficients using the CD data from each WUCD operation. This is different from C6.1 in that the pre-launch  $a_0$  coefficients (with instrument temperature adjustment) used have no bias correction, and the  $a_2$  coefficients are the pre-launch  $a_2$  coefficients adjusted using an iteration procedure described by Wu et al. [2]. There was no algorithm change to the band 21  $b_1$  coefficients (linear fit with  $a_0$  and  $a_2$  equal to zero). Using C7 test LUTs, selected EV targets were evaluated by producing C7 test L1B data to compare with the official C6.1 L1B product. Figure 4.3-4 displays the mirror side BT differences between the C6.1 L1B and C7 test LUT L1B products for Aqua MODIS TEB 22, 23, 27, and 30. The MODIS retrievals are analyzed by cross-comparing with results from the AIRS instrument also onboard Aqua. All data are from September 17<sup>th</sup>, 2017. The results indicate significant reduction in mirror side differences for the bands shown. Moreover, all other bands covered by the AIRS wavelength spectrum demonstrated significant improvement as well. The test results demonstrate significant reduction in mirror side differences for all TEBs - especially for the Aqua MODIS TEBs in C6.1 whose mirror side differences are quite large. After the  $a_0$  bias correction, these MS differences are greatly reduced. Likewise, PV LWIR bands 27-30 show substantial reduction in their MS differences after the correction. Lastly, since the mirror side differences for the PC LWIR bands in C6.1 are marginal, the correction is not applied in C7. A more detailed description of the MODIS TEBs calibration algorithm improvements for C7 is provided by Chang et al. [14].

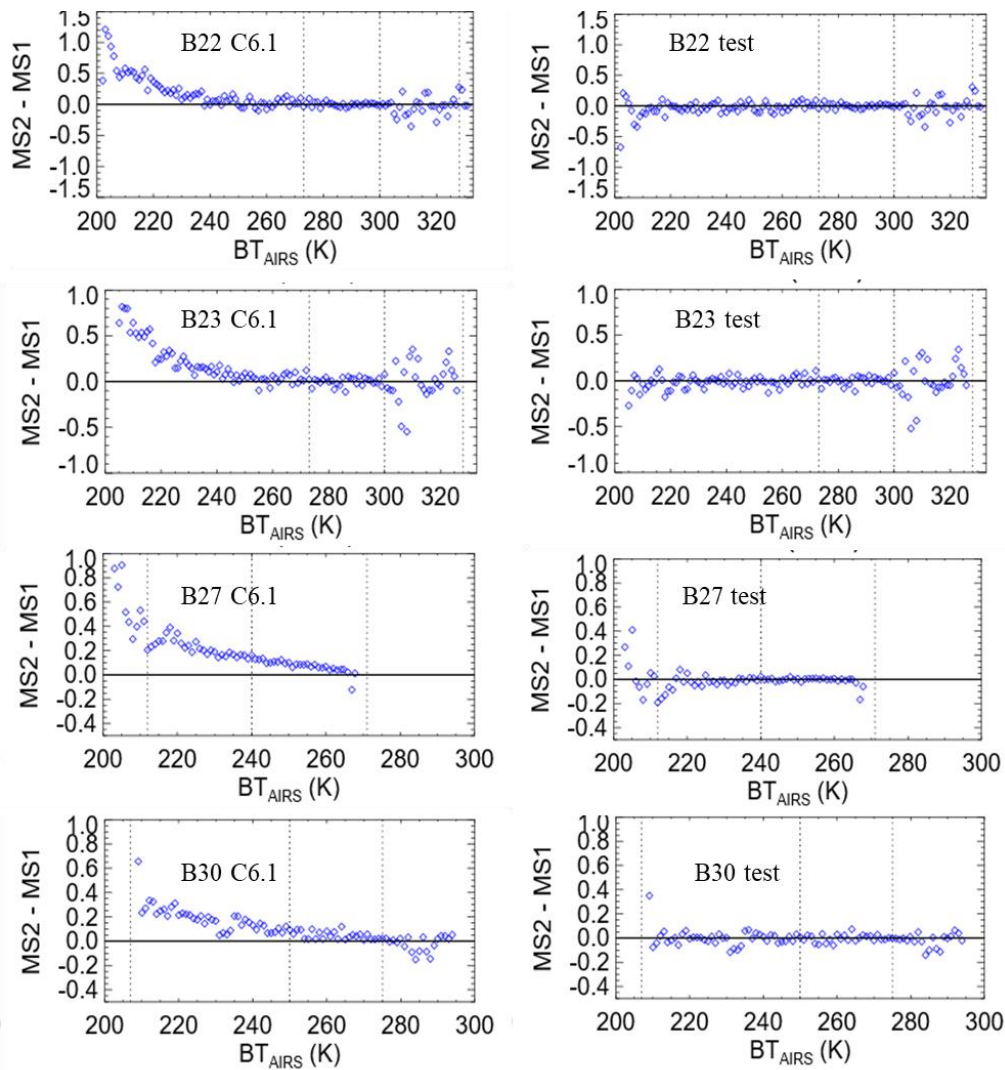


Figure 4.3-4. Aqua MODIS C6.1 L1B and C7 LUT L1B products mirror side BT differences for bands 22, 23, 27, and 30 using an Aqua MODIS-to-AIRS cross-comparison. All data are from September 17, 2017. (Left) C6.1 mirror side BT differences as a function of the AIRS BT for Aqua bands 22, 23, 27, and 30. (Right) C7 mirror side BT differences as a function of the AIRS BT for Aqua bands 22, 23, 27, and 30. The vertical dotted lines represent BTs at 0.3 of typical radiance, typical temperature, and maximum temperature for each TEB from left to right, respectively.

#### 4.4 PV LWIR bands stability improvement

Similar to Terra, the Aqua PV LWIR bands have crosstalk and long-term stability issues. In the C6.1 L1B product, the long-term stability is BT dependent. Over the entire mission, band 29 shows an upward trend, while bands 27, 28, and 30 display downward trends (with band 30 being the largest). Most of these drifts started around year 2012.

The C7 algorithm improvements for PV LWIR drift correction were made in two stages. First, the initial algorithm was developed based on trends in 2020-2021 for the initial C7 LUT delivery made in

March 2021. Second, an updated algorithm was developed based on analysis after the 2022 safe mode which had a large impact on crosstalk for these bands. The updated algorithm was used in the most recent Aqua C7 LUT delivery in November 2023. In this sub-section only, we describe both the initial (referred to as “current” in the table and plots) and the updated algorithms for reference. In the rest of this memo, the tables, plots, and text refer only to the updated algorithm.

The initial C7 calibration algorithm improvements for these bands include crosstalk correction and setting a2 LUT to be fixed after 2012036. For bands 27, 28, and 30, these calibration improvements largely reduce the drift. For band 29, after applications of the crosstalk correction and a2 algorithm, the trending assessments of measurements over Earth scenes show the improvements over warm scenes. However, the Dome-C trending shows a 0.5-K drift over the mission. An additional a0 correction based on this Dome-C drift is generated to improve the trending at low BT Earth scenes for band 29.

After the March 2022 Aqua safe mode, MCST looked extensively at its impacts on the MODIS TEB and found band 29 to be drifting across different scenes. This was due to the fact that electronic crosstalk between the PV LWIR bands has been increasing sharply since 2018, and the algorithm for the non-linear calibration coefficients was fixed to year 2012 after various tests during C7 TEB algorithm definition (back in ~2020-2021; prior to recent crosstalk increase, crosstalk was much smaller then). After thorough analyses, MCST decided to no longer fix the a2 calibration coefficient to its 2012 value for bands 27, 28, and 29. Band 30 continues to be stable and making this change did not prove to benefit the trending. As part of this drifting correction strategy, the band 29 crosstalk coefficients were also amplified by a factor ranging from 0.875 to 1.75 depending on the period in the mission and the impact of the crosstalk on the EV scenes. Overall, the calibration algorithm improvements reduce long-term drifts for all PV LWIR bands over different EV scenes (i.e. tested over DCC, Dome-C, desert, and ocean). Lastly, any residual drifts over colder scenes that remained after these algorithm changes for the PV LWIR bands were then revised by deriving an additional a0 correction from the deep convective clouds trending. This correction was applied back to the C7 LUT, tested, and proved to work properly. Table 4.4-1 recaps the C7 algorithm changes for the Aqua MODIS PV LWIR bands starting year 2012. Figure 4.4-1 shows examples of the improvements these algorithm changes cause over deep convective cloud and ocean scenes for Aqua MODIS bands 27 and 29.

Table 4.4-1. Aqua MODIS C7 PV LWIR bands algorithm changes starting 2012.

Band	Current C7			Updated C7		
	a <sub>0</sub>	a <sub>2</sub>	xtalk	a <sub>0</sub>	a <sub>2</sub>	xtalk
27	PL + MS corr	fixed 2012	All dets and adjusted using EV scenes	PL + MS corr + cold scene drift corr	free-fit using BB CD data	Same as current C7
28						
29	Same + cold scene drift corr				Times 0.875 (2012- 2017), 1.25 (2018-2020), 1.5 (2021-before SM) and 1.75 (after SM), then adjusted	
30	PL + MS corr					fixed 2012

Text in red represents changes from previous C7 algorithm.

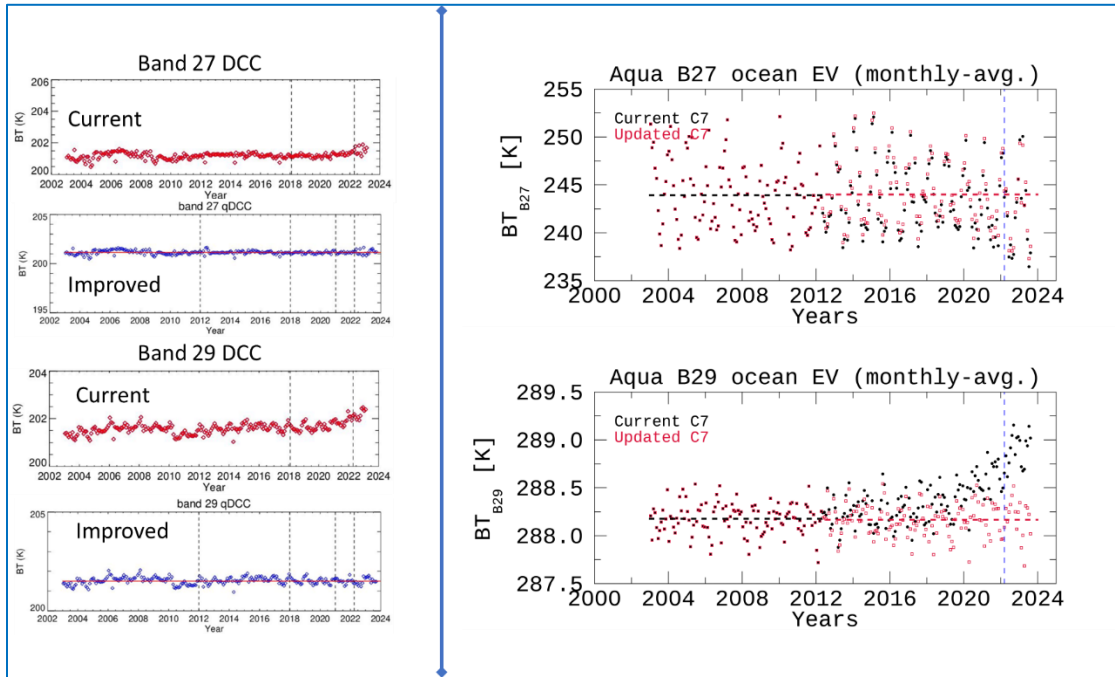


Figure 4.4-1. Examples of the improvements caused by the C7 algorithm changes after 2012 over (left) deep convective cloud and (right) ocean scenes for Aqua MODIS bands 27 and 29.

#### 4.5 PC bands algorithm synopsis

In the initial version of the Aqua C7 LUTs (released in March 2021), the PC bands algorithm was changed relative to C6.1 with the intent to (1) better capture the on-orbit changes seen by the on-board calibrator blackbody and (2) correct marginal mirror side differences seen over cold scenes in C6.1. This was done by applying a deep convective cloud derived  $a_0$  correction to the offset term in the calibration algorithm and deriving the non-linear  $a_2$  term using the cooldown data obtained from the quarterly scheduled blackbody warm-up and cooldown operations. As summarized in Table 1.2-2, the Aqua C6.1 algorithm for these bands is different: the  $a_0$  term is set to zero, while the  $a_2$  term comes from prelaunch and is adjusted using on-orbit data. However, after several discussions with the science teams, a message was conveyed to keep the C6.1 algorithm after various science tests showed significant differences between their C6.1 and C7 cloud products. Thus, MCST made the decision to keep the C6.1 algorithm for the PC bands in the most recent version of the C7 LUTs (delivered in November 2023), while all other bands will have the C7 algorithm implemented (Table 1.2-2).

### 5. SUMMARY

The MCST TEB group has proposed updates for C7 based on a thorough review of the C6.1 TEB LUT algorithm and delivery procedure, and calibration assessments using Earth scenes and sensor inter-comparisons. This document provides a point-by-point discussion associated with each proposed algorithm improvement. Based on the internal test results, MCST expects an improved radiometric

accuracy and quality of the C7 L1B. This memo only includes the discussion pertaining to the changes proposed to the LUTs in C7. Moreover, all LUTs are expected to be reprocessed using the most recent data and procedures.

## REFERENCES

- [1] Xiong, X., A. Wu, B. N. Wenny, S. Madhavan, Z. Wang, Y. Li, N. Chen, W. Barnes, and V. Salomonson, "Terra and Aqua MODIS Thermal Emissive Bands On-Orbit Calibration and Performance", *IEEE Transactions on Geoscience and Remote Sensing*, vol. 53, issue 10, pp. 5709 - 5721, 2015.
- [2] Wu, A., Z. Wang, Y. Li, S. Madhavan, B. N. Wenny, N. Chen, and X. Xiong, "Adjusting Aqua MODIS TEB nonlinear calibration coefficients using iterative solution," *Proc. SPIE 9264, Earth Observing Missions and Sensors: Development, Implementation, and Characterization III*, 92640R (2 December 2014); <https://doi.org/10.1117/12.2069246>.
- [3] Sun, J., X. Xiong, Y. Li, S. Madhavan, A. Wu, and B. N. Wenny, "Evaluation of Radiometric Improvements With Electronic Crosstalk Correction for Terra MODIS Band 27", *IEEE Transactions on Geoscience and Remote Sensing*, vol. 52, issue 10, pp. 6497 - 6507, 2014.
- [4] Wilson, T., A. Wu, A. Shrestha, X. Geng, Z. Wang, C. Moeller, R. Frey, and X. Xiong, "Development and Implementation of an Electronic Crosstalk Correction for Bands 27–30 in Terra MODIS Collection 6," *Remote Sens.*, vol. 9, issue 569, 2017.
- [5] MODIS Thermal Emissive Band Crosstalk Workshop. MsWG meeting. August 2018. <https://mcst.gsfc.nasa.gov/meetings/modis-thermal-emissive-band-crosstalk-workshop>.
- [6] Chang, T., X. Xiong, A. Shrestha, and C. Perez Diaz, "Methodology development for calibration assessment using quasi-deep convective clouds with application to Aqua MODIS TEB. *Earth and Space Science*," vol. 7, e2019EA001055, 2020. <https://doi.org/10.1029/2019EA001055>.
- [7] C. Moeller. MODIS and VIIRS TEB Performance. MCST and VCST Calibration Workshop 2019. November 2019. [https://mcst.gsfc.nasa.gov/sites/default/files/meetings\\_files/03\\_Moeller\\_TEBVIIRS.pdf](https://mcst.gsfc.nasa.gov/sites/default/files/meetings_files/03_Moeller_TEBVIIRS.pdf).
- [8] Li Y., A. Wu, and X. Xiong, "Assessment of MODIS collection 6.1 thermal emissive band calibration using hyperspectral IASI observations," *Proc. SPIE 11530, Sensors, Systems, and Next-Generation Satellites XXIV*, 1153019 (20 September 2020); <https://doi.org/10.1117/12.2571488>.
- [9] Chang, T., X. Xiong, and A. Angal, "Terra and Aqua MODIS TEB intercomparison using Himawari-8/AHI as reference", *Journal of Applied Remote Sensing*, vol. 13, issue 1, pp. 017501, 2019.
- [10] Pérez Díaz, C., X. Xiong, and A. Wu, "MODIS thermal emissive bands calibration stability using in-situ ocean targets and remotely-sensed SST retrievals provided by the group for high resolution sea

surface temperature," Proc. SPIE 11014, Ocean Sensing and Monitoring XI, 110140P (10 May 2019); <https://doi.org/10.1117/12.2518691>.

[11] Xiong, X., A. Shrestha, and B. Wenny, "Assessments of MODIS thermal emissive bands on-orbit calibration performance using Dome C observations," Proc. SPIE 10986, Algorithms, Technologies, and Applications for Multispectral and Hyperspectral Imagery XXV, 1098605 (14 May 2019); <https://doi.org/10.1117/12.2519000>.

[12] Keller, G. R., Z. Wang, A. Wu, and X. Xiong, "Aqua MODIS electronic crosstalk survey from Moon observations," Proc. SPIE 10423, Sensors, Systems, and Next-Generation Satellites XXI, 1042314 (29 September 2017); <https://doi.org/10.1117/12.2277972>.

[13] Keller, G. R., T. Wilson, X. Geng, A. Wu, Z. Wang and X. Xiong, "Aqua MODIS Electronic Crosstalk Survey: Mid-Wave Infrared Bands," IEEE Transactions on Geoscience and Remote Sensing, vol. 57, no. 3, pp. 1684-1697, 2019, doi: 10.1109/TGRS.2018.2868613.

[14] Chang, T., A. Shrestha, C. Perez Diaz, Y. Li, N. Chen, A. Wu, X. Xiong, "MODIS TEB calibration algorithm improvements for future L1B collection," Proc. SPIE 11501, Earth Observing Systems XXV, 115011H (20 August 2020); <https://doi.org/10.1117/12.2567226>.

[15] Xiong, X., A. Angal, W. L. Barnes, H. Chen, V. Chiang, X. Geng, Y. Li, K. Twedt, Z. Wang, T. Wilson, et al., "Updates of Moderate Resolution Imaging Spectroradiometer on-orbit calibration uncertainty assessments", Journal of Applied Remote Sensing, vol. 12(3),034001, 2018.

[16] Tiejun Chang, Hanzhi Lin, Carlos Diaz, Xiaoxiong Xiong, "Aqua MODIS TEB crosstalk correction improvement and image quality enhancement," Proc. SPIE 12685, Earth Observing Systems XXVIII, 126851E (4 October 2023); <https://doi.org/10.1117/12.2677395>